Journal of Power Sources 269 (2014) 755–759

Contents lists available at ScienceDirect

Journal of Power Sources

journal homepage: www.elsevier.com/locate/jpowsour

Short communication

High cycleability nano-GeO_2/mesoporous carbon composite as enhanced energy storage anode material in Li-ion batteries

Ali Jahel [a, b, c], Ali Darwiche [a, c], Camélia Matei Ghimbeu [b, c, *], Cathie Vix-Guterl [b, c], Laure Monconduit [a, c]

[a] ICG/AIME (UMR 5253 CNRS), Université Montpellier II CC 15-02, Place E. Bataillon, 34095 Montpellier Cedex 5, France
[b] Institut de Science des Matériaux de Mulhouse (IS2M), UMR 7361 CNRS, 15 rue Jean Starcky, BP 2488, 68057 Mulhouse Cedex, France
[c] Réseau sur le Stockage Electrochimique de l'Energie (RS2E), CNRS FR3459, 33 Rue Saint Leu, 80039 Amiens Cedex, France

HIGHLIGHTS

- Mesoporous carbon with confined GeO_2 nanoparticles is prepared by a simple approach.
- The composite shows exceptional capacity retention (93%) at 1 C after 380 cycles.
- The composite exhibits high rate capability at variable current rates.
- Low amounts of GeO_2 in carbon provide high coulombic efficiency and long cycle life.
- GeO_2 morphological restructuration during the first cycles decreases their size.

ARTICLE INFO

Article history:
Received 23 April 2014
Received in revised form
30 June 2014
Accepted 8 July 2014
Available online 17 July 2014

Keywords:
Li-ion battery
Anode
Germanium
GeO_2
Mesoporous carbon
Nanoconfinement

ABSTRACT

A novel nano-GeO_2/mesoporous carbon (GeO_2/MC) composite material was prepared by *in-situ* decomposition of germanium ethoxide ($Ge(OC_2H_5)_4$) infiltrated in a mesoporous carbon (MC) obtained by soft-templating procedure. With GeO_2 (<20 nm) homogeneously distributed in the carbon network, the GeO_2/MC composite retains 93% of its initial charge capacity after 380 cycles at constant 1 C rate (1500 mA g^{-1}) as electrode material vs. Li and shows high rate capability at variable current rates. A restructuration of the germanium phase into smaller particles during the first cycles is also evidenced. The composite presents a set of advantages such as low GeO_2 content, convenient preparation approach and high coulombic efficiency (>99%).

1. Introduction

Silicon and germanium Li-ion battery anodes have high theoretical capacities (4200 and 1600 mAh g^{-1}, respectively) [1] compared to graphite anodes (372 mAh g^{-1}) [2,3] which have a limited Li storage capacity. Despite its lower theoretical capacity compared to silicon, germanium has higher Li-ion diffusivity than silicon (almost 400 times), higher electric conductivity (10^4 times) [4,5] and slightly lower specific volume change during lithiation/delithiation. However during repetitive Li insertion/extraction in germanium it can still undergo pulverization and capacity loss due to volumic expansion during cycling [6,7]. Moreover, germanium is more expensive than common metal oxides which represent a drawback. Several approaches were proposed to enhance germanium performances including mainly morphology modifications strategies i.e., nanoparticles, [5,8] nanowires, [9,10] and nanotubes, [11] or association of germanium with other materials to form germanium-based composites (tin–germanium, [12] germanium/carbon nanotubes [13]), germanium oxides, [14] and germanium/graphene [15]. Although these materials present several advantages, the amount of expensive germanium used is still high, and their preparation procedure is relatively complicated. Ordered mesoporous carbons obtained by hard-templating (with SBA-15) and soft-templating (using triblock copolymers) have been

* Corresponding author. Institut de Science des Matériaux de Mulhouse (IS2M), UMR 7361 CNRS, 15 rue Jean Starcky, BP 2488, 68057 Mulhouse Cedex, France. Tel.: +33 (3) 89 60 87 43; fax: +33 3 89 60 87 99.
E-mail address: camelia.ghimbeu@uha.fr (C. Matei Ghimbeu).

http://dx.doi.org/10.1016/j.jpowsour.2014.07.042
0378-7753/

recently employed to enhance cycling performances of Sn and SnO_2 [16–19], sulfur [20] and phosphorous [21] electrodes. The advantages of using mesoporous carbons are basically related to their good conductivity, open interconnected porosity allowing the insertion of such electrode species but also enhancing the electrolyte diffusion. Herein, we report a simple, environmentally friendly preparation of a GeO_2/mesoporous carbon composite (GeO_2/MC) by simple infiltration of $Ge(OC_2H_5)_4$ in a high surface area micro-mesoporous carbon (obtained by soft-templating). The characteristics of this composite were determined by several analysis techniques (N_2 adsorption, Transmission Electron Microscopy (TEM), X-ray diffraction (XRD)) while the electrochemical performances were tested in coin cells vs. Li/Li^+. The composite containing low amount of germanium oxide (~40wt.%) demonstrated excellent capacity retention after 380 cycles (93%) and high rate capability. This may result from the nanoconfinement of GeO_2 particles inside the carbon matrix preventing particle coalescence and electrode pulverization.

2. Experimental

2.1. Materials synthesis

The micro-mesoporous carbon framework was prepared via soft-templating method involving self-assembly of environmentally friendly phloroglucinol and glyoxal carbon precursors with a triblock copolymer template followed by thermal treatment. [22] GeO_2/MC composite was prepared by impregnation of the carbon with diluted $Ge(OC_2H_5)_4$. The surface of the mesoporous carbon was functionalized by contact with H_2O_2 in order to increase the quantity of oxygenated functional groups and improve the hydrophilic character [23]. After washing with distilled water, filtration and drying (80 °C, 12 h), the carbon was placed in absolute ethanol (5 ml) and $Ge(OC_2H_5)_4$ (≥99.5%, Sigma Aldrich) was slowly added (20 wt.% solution in absolute ethanol) while stirring. The slurry was left under agitation until complete ethanol evaporation and the obtained powder was dried overnight at 90 °C and subsequently heated at 350 °C during 2 h under argon to decompose $Ge(OC_2H_5)_4$.

2.2. Materials characterization

Thermogravimetric analysis (TGA) was conducted on a TGA 851 (Mettler-Toledo) thermogravimeter by heating the sample under air (100 ml min^{-1}) up to 900 °C with a 5 °C min^{-1} rate allowing the combustion of carbon and the determination of germanium oxide residue. The GeO_2 loading in the final composite was found to be 40 wt.% (Fig. S1, Supporting information). The crystalline structure of the products was characterized by X-ray powder diffraction (XRD) with a Philips PCW30 diffractometer using CuKα radiation. Transmission electron microscopy (TEM) experiments were performed on a Philips CM200 microscope working at 200 kV. The long-range ordering of the materials was studied by Small Angle X-ray Scattering (SAXS) (Fig. S2) analysis using a RigakuSMax 3000 equipped with a rotating Cu anode Micromax-007HF (40 kV, 30 mA) and OSMIC CMF optics. The detector is a 2D multiwires Gabriel chamber with 120 mm active diameter. Nitrogen adsorption isotherms were measured at −196 °C on a Micromeritics ASAP 2024 apparatus. The samples were out-gassed in vacuum at 200 °C during 10 h before starting the measurements. The Brunauer–Emmett–Teller (BET) method was used to determined the specific surface areas. The pore size distributions were derived from the desorption branches of the isotherms using the Barrett–Joyner–Halenda (BJH) model. The total porous volume (V_T) was estimated at a relative pressure of 0.95.

2.3. Electrochemical characterization

Electrochemical performance of the GeO_2/MC composite electrode was investigated in coin cells at a current density of 1 C (1500 mA g^{-1}) in the voltage range of 0.01–1.5 V (vs. Li/Li^+) with Mac pile (Biologic SA) battery testing system. The electrode mixture was made by mixing as prepared GeO_2/MC composite, carbon black, and binder (carboxymethylcellulose, CMC) at a mass ratio of 80:10:10. Subsequently, it was dispersed in pure water and ground to obtain a homogeneous mixture. Then, the slurry was coated uniformly onto a 25 μm thick copper foil with a diameter of 14 mm using a doctor blade and dried at 100 °C for 12 h in vacuum. Coin cells were assembled in argon filled glove box. The electrolyte was 1 M $LiPF_6$ in a mixture containing ethylene carbonate (EC), propylene carbonate (PC), dimethyl carbonate (DMC) (1:1:3 in weight), with 2 wt.% vinyl carbonate (VC) and 10 wt.% Fluoroethylene carbonate (FEC). Fluorinated additives such as FEC and VC have been reported to play an important role in promoting the electrochemical performance of germanium [24–26].

3. Results and discussion

All peaks in the GeO_2/MC composite XRD patterns could be well ascribed to hexagonal phase (ICDD no. 36-1463) GeO_2 (Fig. 1a) with average crystallites size of 20 nm (determined using Scherrer formula). Due to the high crystallinity of the GeO_2 phase well dispersed in the sample, the peaks of the starting mesoporous carbon (Fig. 1d) are no longer observed in the GeO_2/MC composite.

TEM pictures (Fig. 1-e,f), show the mesoporous carbon which exhibit a rather worm like structure. However, the SAXS patterns reveals a small peak near 0.7° (Fig. S2 in supporting information) indicating a certain degree of ordered hexagonal morphology in the material, in line with our previous reports [19,22]. TEM (Fig. 1-b,c) shows that GeO_2 is present as small particles (5–20 nm) gathered in agglomerates with about 50 nm size homogeneously dispersed in the carbon matrix, in agreement with XRD results. GeO_2 agglomerates appear to be well embedded inside the mesopores and therefore present a morphology that follows that of the carbon framework.

The textural properties of materials before and after the GeO_2 insertion were evaluated using N_2 adsorption/desorption isotherms presented in Fig. 2. The mesoporous carbon presents a high specific surface area (705 m^2 g^{-1}) and a high porous volume (1.06 cm^3 g^{-1}) with microporous volume of 0.3 cm^3 g^{-1}. The GeO_2/MC composite's surface area (302 m^2 g^{-1}) and porous volume (0.40 cm^3 g^{-1}) are ~60% lower compared to carbon alone, indicative of pore filling by GeO_2. Carbon material and GeO_2/MC composite have similar narrow pore distributions and BJH average pore diameter centered around 8 nm (in-set Fig. 2), in accordance with our previous reports [19,22]. Some microporous volume is still available (0.14 cm^3 g^{-1}) in the composite.

Fig. 3a shows the galvanostatic cyclic performance of the GeO_2/MC composite at constant 1 C rate in [0.01–1.5 V] range. The initial discharge/charge capacities of the composite are 1380 and 492 mAh g^{-1} respectively corresponding to an initial coulombic efficiency (CE) of only 36%. This can be also supported by the galvanostatic curve of the GeO_2/MC composite (Fig. S3 in Supporting information). The large irreversible initial capacity can be attributed to irreversible insertion of lithium in the porous carbon and to the formation of a massive solid electrolyte interface (SEI) due to the high surface area. This is previously reported and common to mesoporous carbons. [16–19]. Irreversibility also results from irreversible formation of $(Li_2O)_yGeO_2$ and Li_2O [27] before transformation into a Ge/Li_2O nanocomposite and LiGe during the first reduction. Indeed, the broad peak centered at 0.7 V is attributed to the formation of Li_xGeO_2 and to the decomposition of the

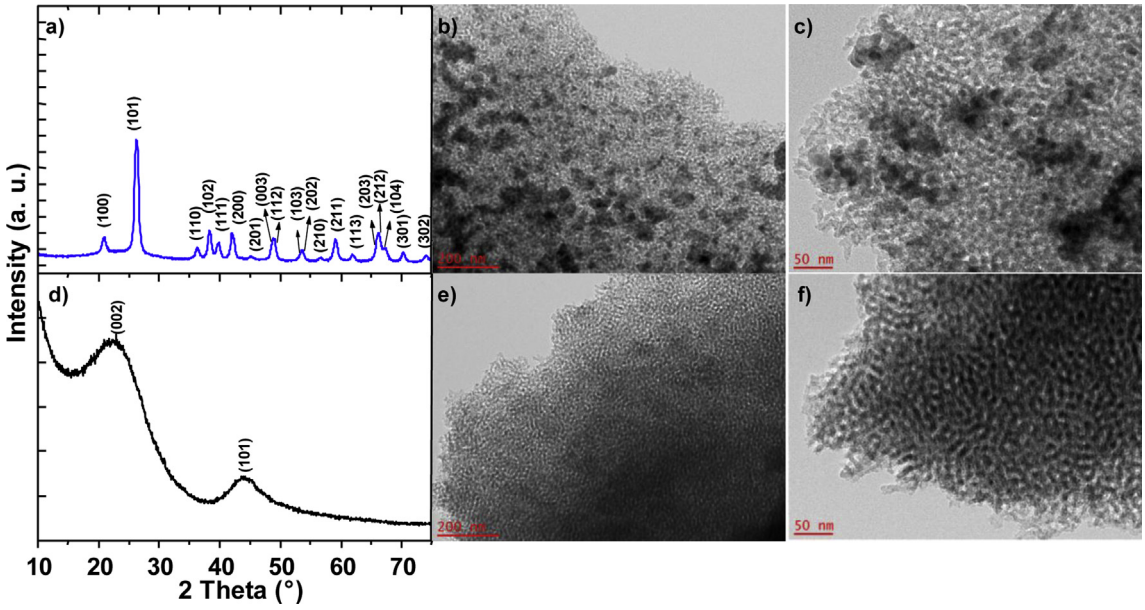

Fig. 1. a) XRD patterns of GeO_2/MC composite, b,c) corresponding TEM images, d) XRD patterns of mesoporous carbon and e,f) corresponding TEM images.

electrolyte to form SEI layer. [24]. The second sharp irreversible feature at 0.41 V can be attributed to reduction of GeO_2 and Li_xGeO_2 into Ge and Li_2O. Decomposition of FEC species to form an irreversible SEI layer has been also reported to occur at a similar voltage [24]. Lithium rich Li_xGe alloys such as Li_7Ge_2, $Li_{15}Ge_4$, $Li_{11}Ge_6$, Li_9Ge_4, and $Li_{22}Ge_5$ are generally formed at lower potential between 0.01 and 0.34 V (Fig. 3b). [28–30]. The dx/dV profile during the first discharge of the GeO_2/MC composite shows three features at low voltage indicating formation of Li_xGe alloys (Fig. 3b). The first feature lies in the 0.2–0.3 V range. This supports the formation of Li_7Ge_3 and Li_5Ge_2 phases. [31] The second feature lies in

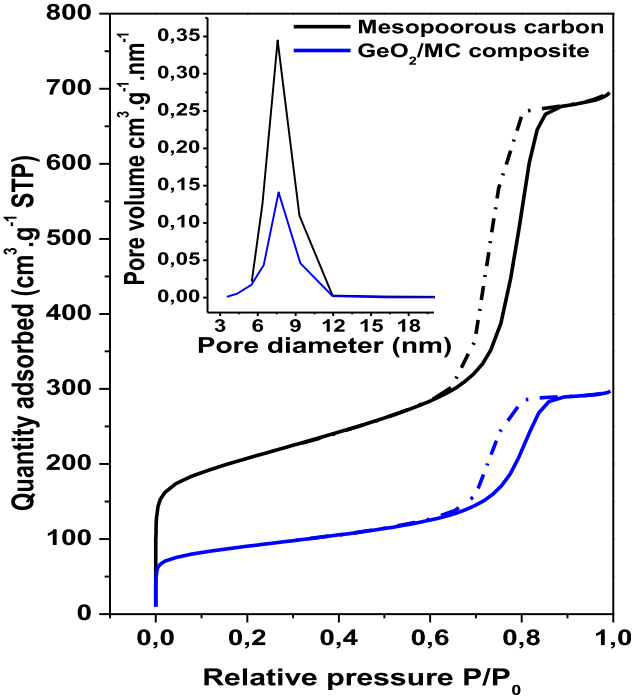

Fig. 2. N_2 adsorption/desorption isotherm of carbon and the GeO_2/MC composite; inset: BJH pore size distribution curve.

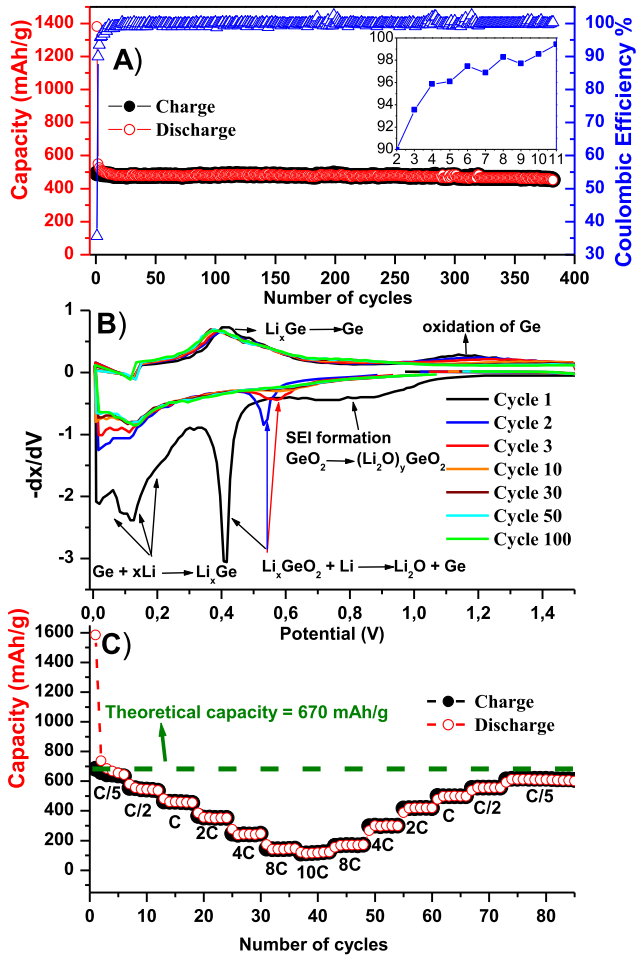

Fig. 3. a) Cycling performance of GeO_2/MC composite at constant rate 1 C (1500 mA g^{-1}), b) derivative galvanostatic $-dx/dV$ profiles at 1 C rate and c) cycling performance of GeO_2/MC composite at variable rate.

the 0.09–0.2 V range and can be attributed to the formation of Li_7Ge_2 phase. [31] These two features can be attributed to two-step mechanisms through which Li is inserted in the Ge crystal lattice [30]. The last feature (Fig. 3b) during discharge occurs at low voltages (0.02–0.09 V) and can be attributed to the formation of ultimate thermodynamically accessible phases such as $Li_{15}Ge_4$ [24]. This can be also supported by the galvanostatic curve of the GeO_2/MC composite (Fig. S3, Supporting information). Yoon et al. [32] studied the Li-insertion mechanism in germanium–carbon composites and reported two distinct voltage plateaus corresponding to the formation of Li_9Ge_4 and Li_7Ge_2, and the final products were identified as a mixture of $Li_{15}Ge_4$ and $Li_{22}Ge_5$ phases. A three-step reaction mechanism of germanium with lithium was suggested. The voltage profile of the GeO_2/MC composite shows, as indicated above, a similar three step mechanism indicating that final insertion products in this study most likely correspond to a mixture of $Li_{15}Ge_4$ and $Li_{22}Ge_5$ as well. These results indicate the efficient usage of the Ge content in the composite with the formation of rich Li_xGe phases. For the first charge (oxidation), a very broad peak centered at 0.36 V and another centered at 1.1 V can be tentatively attributed to delithiation of the Li_xGe alloys and some oxidation of Ge, respectively. [33] Coulombic efficiency (CE) rises in the second cycle to 90% as less SEI is formed and as oxidic phases have been quite irreversibly reduced during first discharge, in agreement with the disappearance of the broad peak between 0.6 and 1.0 V. However, during the second discharge a new less intense peak is observed at 0.53 V, which might be attributed to reduction of remaining GeO_2 phase or reoxidized Ge during the first charge (oxidation). This increase in potential of the first plateau between the first and second discharge resembles to that observed for conversion-type materials (either vs. Li or Na), with a first characteristic discharge at lower potential than the following ones. This reduction of the polarization is due to the restructuration and the decrease of the particle size, classically called “electro-chemical grinding” of the starting material during the first discharge. [34] Delithiation of Li_xGe during the second charge (oxidation) occurs with an equally intense broad peak near 0.36 V. The small reduction peak occurring at 0.53 V in the second discharge is further shifted to 0.57 V with some broadening and further intensity loss, meaning that reoxidation of Ge during the second charge and electrochemical grinding are now more limited, and CE reaches 94% (inset Fig.3a). Starting with the fourth cycle (not shown), this peak is no longer seen, suggesting that the first three discharges cause electrochemical restructuration of the starting material to form the effective electrode material. The profiles at 10, 30, 50 and 100 cycles are quite identical, indicating a stable lithiation/delithiation process in agreement with stable capacity. CE reaches more than 99% starting from the 10th cycle (inset Fig. 3a). The charge capacity retained after 380 cycles at constant 1 C rate is equal to 452 mAh g^{-1}, corresponding to 93% retention of the initial capacity (492 mAh g^{-1}) and demonstrating the excellent cyleability of the composite. Rate capability is also shown in Fig. 3c. The initial reversible charge capacity of the composite is 680 mAh g^{-1} at 0.2 C, slightly higher than the theoretical capacity of the composite (670 mAh g^{-1}) indicating full germanium usage. It reaches 550, 480, 364, 246, 144 and 120 mAh g^{-1} at 0.5 C, C, 2 C, 4 C, 8 C and 10 C, respectively. The composite almost fully recovers its charge capacity upon decreasing the current density, reaching 612 mAh g^{-1} after 75 cycles at 0.2 C, (90% of its initial charge capacity). C. Yao et al. [35] reported similar Ge/C composites obtained by germanium ethoxide ($Ge(OC_2H_5)_4$) impregnation on mesoporous carbon and further reduction in H_2 to obtain Ge/C composite. However, the size of obtained particles is relatively high (about 200 nm) compared to 20 nm in our current work. Our impregnation method involving carbon surface chemistry modification and impregnation

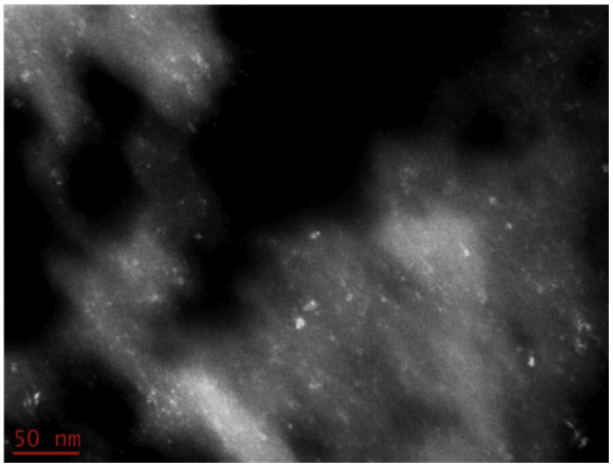

Fig. 4. TEM image of GeO_2/MC composite after 380 cycles at 1 C rate.

in excess ethanol certainly leads to better dispersion of GeO_2 particles. The GeO_2/MC composite in this work only contains 27.7 wt.% of elemental Ge and its capacity and capacity retention after 380 cycles are significantly enhanced (460 mAh g^{-1} after 380 cycles at 1.5 A g^{-1} rate compared to 237 mAh g^{-1} after 20 cycles at 0.1 A g^{-1} rate reported by C. Yao et al. [35]. TEM imaging of GeO_2/MC composite after 380th cycles (Fig. 4) reveals small particles (<6 nm size). Larger aggregates (size = 50 nm) seen before cycling (Fig 1b) can no longer be observed, in line with previous observations. Most of active phase particles therefore have sizes lower than the average pore size of the mesopores, and these particles are most probably confined inside the pores, explaining their high stability and the absence of particle coalescence even after 380 cycles. So far, reports on amorphous Ge nanoparticles show good cycleability and capacity retention only during the first 50th cycles. [5] Similarly, we have recently reported [19] that confinement of SnO_2 nanoparticles (2.8 nm average) inside carbon mesopores leads to much more stable anodes compared to unconfined nanoparticles even for very low particle sizes (3 nm). Decreasing the particle size (<10 nm) is beneficial only if combined with confinement inside carbon mesopores. This is ascribed to the accomodation of volume changes during cycling inside mesopores, and to the enhancement of electrolyte transport via the open interconnected micro-mesopores in the composite. [19] Our present work demonstrates a similar promoting role of mesoporous carbons for Ge based materials. However as in all carbon-based composites, the irreversibility during first discharge (Fig. S3, Supporting Information) remains the main drawback to be overcome.

4. Conclusions

A facile synthesis route of novel confined GeO_2 in micro-mesoporous carbon as anode material for Li-ion batteries is reported. GeO_2/MC composite has GeO_2 particles in the 5–20 nm range which decreases significantly during the first three cycles vs. Li due to the electrochemical grinding. This affords an excellent cycleability of the GeO_2/MC composite, retaining 93% of its initial capacity (492 mAh g^{-1}) after 380 cycles at 1 C rate (1500 mA g^{-1}), and good rate capability up to 10 C. Electrochemical nanostructuration which occurs during first cycles assure accommodation of volume changes inside mesopores upon cycling. This is well corroborated with the good electric conductivity of carbon and its ordered interconnected pores facilitating the electrolyte diffusion, the GeO_2/MC composite exhibit performances largely exceeding similar reported GeO_2/C composites. Nevertheless, the composite

also presents the advantages of low GeO_2 content and high CE (>99%).

Acknowledgements

The RS2E (Réseau sur le Stockage Electrochimique de l'Energie) network is aknowledged for the financial support of this work through the ANR project Storex (ANR-10-LABX-76-01). Dr. Loïc Vidal and Gautier Schrodj (IS2M) are acknowledged for the help with TEM and TGA measurements.

Appendix A. Supplementary data

Supplementary data related to this article can be found at http://dx.doi.org/10.1016/j.jpowsour.2014.07.042.

References

[1] W.J. Weydanz, M. Wohlfahrens-Mehrens, R.A. Huggins, J. Power Sources 81 (2003) 237.
[2] J.R. Dahn, T. Zheng, Y. Liu, J.S. Xue, 270 (1995) 590.
[3] M.S. Dresselhaus, G. Dresselhaus, Adv. Phys. 30 (1981) 139.
[4] D. Wang, Y.L. Chang, Q. Wang, J. Cao, D.B. Farmer, R.G. Gordon, H. Dai, J. Am. Chem. Soc. 126 (2004) 11602.
[5] H. Lee, M.G. Kim, C.H. Choi, Y. Sun, C.S. Yoon, J. Cho, J. Phys. Chem. B 109 (2005) 20719.
[6] M. Winter, J.O. Bsenhard, Electrochim. Acta 45 (2000) 31.
[7] L.Y. Beaulieu, J.R. Dahn, J. Electrochem. Soc. 147 (2000) 3237.
[8] G.L. Cui, L. Gu, L.J. Zhi, N. Kaskhedikar, P.A. Van Aken, K. Mullen, J. Maier, Adv. Mater. 20 (2008) 3079.
[9] C.K. Chan, X.F. Zhang, Y. Cui, Nano Lett. 8 (2008) 307.
[10] Y.D. Ko, J.G. Kang, G.H. Lee, J.G. Park, K.S. Park, Y.H. Jin, D.W. Kim, Nanoscale 3 (2011) 3371.
[11] M.H. Park, Y. Cho, K. Kim, J. Kim, M.L. Liu, J. Cho, Angew.Chem. Int. Ed. 123 (2011) 9821.
[12] M.G. Kim, J. Cho, J. Electrochem. Soc. 156 (2009) A277.
[13] R.A. DiLeo, S. Frisco, M.J. Ganter, R.E. Rogers, R.P. Raffaelle, B.J. Landi, J. Phys. Chem. C 115 (2011) 22609.
[14] X.-L. Wang, W.-Q. Han, H. Chen, J. Bai, T.A. Tyson, X.-Q. Yu, X.-J. Wang, X.-Q. Yang, J. Am. Chem. Soc. 133 (2011) 20692.
[15] H. Kim, Y. Son, C. Park, J. Cho, H.C. Choi, Angew.Chem. Int. Ed. 52 (2013) 5997.
[16] F.M. Hassan, Z. Chen, A. Yu, Z. Chen, X. Xiao, Electrochim. Acta 87 (2013) 844.
[17] Y. Wang, B. Li, C. Zhang, H. Tao, S. Kang, S. Jiang, X. Li, J. Power Sources 219 (2012) 89.
[18] Y. Xu, Y. Guo, C. Wang, J. Mater. Chem. 22 (2012) 9562.
[19] A. Jahel, C. Matei Ghimbeu, L. Monconduit, C. Vix-Guterl, Adv. Energ. Mater. http://dx.doi.org/10.1002/aenm.201400025.
[20] X. Ji, K.L. Tae, L.F. Nazar, Nat. Mater. 8 (2009) 500.
[21] C. Marino, A. Debenedetti, B. Fraisse, F. Favier, L. Monconduit, Electrochem. Commun. 13 (2011) 346.
[22] C. Matei-Ghimbeu, J.-M. Le Meins, C. Zlotea, L. Vidal, G. Schrodj, M. Latroche, C. Vix-Guterl, Carbon 67 (2014) 260.
[23] C. Matei-Ghimbeu, R. Gadiou, J. Dentzer, D. Schwartz, C. Vix-Guterl, Langmuir 26 (2010) 18824.
[24] H.A. Wilhelm, C. Marino, A. Darwiche, L. Monconduit, B. Lestriez, Electrochem. Commun. 24 (2012) 89.
[25] L. El Ouatani, R. Dedryvère, C. Siret, P. Biensan, D. Gonbeau, J. Electrochem. Soc. 156 (2009) A468.
[26] K.C. Klavetter, S.M. Wood, Y.-M. Lin, J.L. Snider, N.C. Davy, A.M. Chockla, D.K. Romanovicz, B.A. Korgel, J.-W. Lee, A. Heller, C.B. Mullins, J. Power Sources 238 (2013) 123.
[27] J.S. Pena, I. Sandu, O. Joubert, F.S. Pascual, C.O. Arean, T. Brousse, Electrochem. Solid State Lett. 7 (2004) A278.
[28] J. Graetz, C.C. Ahn, R. Yazami, B. Fultz, J. Electochem. Soc. 151 (2004) A698.
[29] L. Baggetto, P.H.L. Notten, J. Electrochem. Soc. 156 (2009) A169.
[30] A.S. Jing Li, R.J. Sanderson, T.D. Hatchard, R.A. Dunlap, J.R. Dahn, J. Electrochem. Soc. 156 (2009) A283.
[31] A.F. Sammells, M.R.St. John, US Patent 4346152, 1982.
[32] S. Yoon, C.-M. Park, H.-J. Sohn, Electrochem. Solid State Lett. 11 (2008) A42.
[33] K.H. Seng, M. Park, Z.P. Guo, H.K. Liu, J. Cho, Nano Lett. 13 (2013) 1230.
[34] A. Darwiche, M.T. Sougrati, B. Fraisse, L. Stievano, L. Monconduit, Electrochem. Commun. 32 (2013) 18.
[35] C. Yao, J. Wang, H. Bao, Y. Shi, Mater. Lett. 124 (2014) 73.